Editors' Suggestion

Orbital Complexity in Intrinsic Magnetic Topological Insulators $MnBi_4Te_7$ and $MnBi_6Te_{10}$

R. C. Vidal,[1,2] H. Bentmann,[1,2,*] J. I. Facio,[3] T. Heider,[4] P. Kagerer,[1,2] C. I. Fornari,[1,2] T. R. F. Peixoto,[1,2] T. Figgemeier,[1,2] S. Jung,[5,6] C. Cacho,[5] B. Büchner,[2,3,7] J. van den Brink,[2,3,7] C. M. Schneider,[4] L. Plucinski,[4] E. F. Schwier,[1,2,8] K. Shimada,[8] M. Richter,[3,9] A. Isaeva,[2,3,7,10] and F. Reinert[1,2]

[1]*Experimentelle Physik VII, Universität Würzburg, Am Hubland, D-97074 Würzburg, Germany, EU*
[2]*Würzburg-Dresden Cluster of Excellence ct.qmat, Germany, EU*
[3]*Leibniz Institute for Solid State and Materials Research (IFW) Dresden, Helmholtzstr. 20, D-01069 Dresden, Germany, EU*
[4]*Peter Grünberg Institut, Forschungszentrum Jülich and JARA, 52425 Jülich, Germany, EU*
[5]*Diamond Light Source, Harwell Campus, Didcot OX11 0DE, United Kingdom*
[6]*Department of Physics, Gyeongsang National University, Jinju 52828, Korea*
[7]*Institut für Festkörper- und Materialphysik, Technische Universität Dresden, D-01062 Dresden, Germany, EU*
[8]*Hiroshima Synchrotron Radiation Center, Hiroshima University, Higashi-Hiroshima, Hiroshima 739-0046, Japan*
[9]*Dresden Center for Computational Materials Science (DCMS), Technische Universität Dresden, D-01062 Dresden, Germany, EU*
[10]*Van der Waals—Zeeman Institute, Institute of Physics, University of Amsterdam, 1098 XH Amsterdam, The Netherlands, EU*

(Received 18 June 2020; revised 9 January 2021; accepted 17 March 2021; published 28 April 2021; corrected 19 May 2021 and 23 September 2021)

Using angle-resolved photoelectron spectroscopy (ARPES), we investigate the surface electronic structure of the magnetic van der Waals compounds $MnBi_4Te_7$ and $MnBi_6Te_{10}$, the $n = 1$ and 2 members of a modular $(Bi_2Te_3)_n(MnBi_2Te_4)$ series, which have attracted recent interest as intrinsic magnetic topological insulators. Combining circular dichroic, spin-resolved and photon-energy-dependent ARPES measurements with calculations based on density functional theory, we unveil complex momentum-dependent orbital and spin textures in the surface electronic structure and disentangle topological from trivial surface bands. We find that the Dirac-cone dispersion of the topologial surface state is strongly perturbed by hybridization with valence-band states for Bi_2Te_3-terminated surfaces but remains preserved for $MnBi_2Te_4$-terminated surfaces. Our results firmly establish the topologically nontrivial nature of these magnetic van der Waals materials and indicate that the possibility of realizing a quantized anomalous Hall conductivity depends on surface termination.

DOI: 10.1103/PhysRevLett.126.176403

Realizing new quantum states of matter based on the interplay of nontrivial band topologies and magnetism is a central goal in modern condensed matter physics [1–5]. A case in point is the magnetic topological insulator (MTI) which combines an inverted electronic band structure with long-range magnetic order [1], providing a promising material platform for the quantum anomalous Hall (QAH) effect, axion electrodynamics, and the topological magnetoelectric effect [2,6–8]. Over the past years, efforts to realize MTI mainly relied on doping of known topological insulators with magnetic impurities [2,6]. Recently, however, so-called intrinsic MTI, which do not require doping, have been discovered in the $MnBi_2Te_4$ class of magnetic van der Waals compounds [4,9–16]. At the same time, $MnBi_2Te_4$ constitutes the first instance of an antiferromagnetic topological insulator [4]. In accordance with theoretical predictions [17,18], recent magnetotransport experiments on two-dimensional few-layer flakes of $MnBi_2Te_4$ revealed signatures of the QAH effect [19] and an axion insulator state [20]. In view of these developments, $MnBi_2Te_4$ and related compounds presently receive broad interest as a platform for the study of quantized magnetoelectric phenomena [21,22].

$MnBi_2Te_4$ constitutes the progenitor of a modular $(Bi_2Te_3)_n(MnBi_2Te_4)$ series of stacked van der Waals compounds [23,24]. Interestingly, the structural incorporation of nonmagnetic Bi_2Te_3 layers alters the magnetic interlayer interactions, resulting in more complex magnetic phase diagrams [5,24–27]. In turn, this provides additional flexibility to manipulate the electronic topology via the magnetic state, which will be crucial to realize recent proposals of exotic electronic phenomena in these systems, such as Majorana modes [28], a higher-order Möbius insulator [29], and a time-reversal-broken quantum spin Hall (QSH) state [30]. Evidence for topological surface states in $MnBi_4Te_7$ and $MnBi_6Te_{10}$ has been reported based on angle-resolved photoelectron spectroscopy (ARPES) [14,25–27,31–38]. However, the assignment of topologically trivial and nontrivial features in the complex, termination-dependent surface electronic structure is still controversial.

Moreover, the helical nature and spin-momentum locking of the surface states, forming the basis of the exotic surface phenomena associated with topological surface states, has not been demonstrated for different terminations.

In this work, we investigate the electronic structure of $MnBi_4Te_7$ and $MnBi_6Te_{10}(0001)$ surfaces by use of circular dichroic, spin-resolved and photon-energy-dependent ARPES measurements. Our results reveal helical spin and orbital textures of the topological surface states (TSS) for different surface terminations. For $MnBi_2Te_4$-terminated surfaces we observe a single Dirac-cone surface state, while for Bi_2Te_3-terminated surfaces hybridization with valence band states strongly modifies the TSS dispersion and induces a gaplike feature in the surface spectral density. These findings have direct implications for future efforts to realize the QAH and QSH effects [30] and other exotic topological phenomena [28,29] in $(Bi_2Te_3)_n(MnBi_2Te_4)$ heterostructures. In particular, our results indicate that a half-quantized Hall conductivity can be achieved for $MnBi_2Te_4$-terminated surfaces but not for Bi_2Te_3-terminated surfaces due to surface-bulk hybridization.

High-resolution ARPES measurements with variable light polarization on single-crystals of $MnBi_4Te_7$ and $MnBi_6Te_{10}$ [24] were performed using a laser-based μ-ARPES system ($h\nu = 6.3$ eV) at the Hiroshima synchrotron radiation center (Japan) [39]. Spin-resolved data were obtained using a laser-based ($h\nu = 6.02$ eV) spin-ARPES apparatus at the Peter Grünberg Institute (PGI-6) in Jülich, equipped with an exchange-scattering-based Focus FERRUM spin detector (Sherman function $S = 0.29$) and an MBS A-1 hemispherical energy analyzer with deflector lens. Photon-energy-dependent ARPES experiments were conducted at beam line I05 of the Diamond Light Source (UK) [40]. Further details of the experiments are provided in the Supplemental Material [41]. Throughout the Letter the in-plane momentum direction parallel (perpendicular) to the plane of light incidence (xz plane) is denoted as k_x (k_y).

To describe the surface electronic properties, we perform calculations, based on density functional theory (DFT), of a slab made of four $MnBi_4Te_7$ unit cells with a vacuum of 30 Å. We use the GGA + U method with the generalized gradient approximation (GGA) [42] as implemented in the FPLO code [43,44]. We fix parameters $U = 5.34$ eV and $J = 0$, as in Ref. [4], with atomic-limit double-counting and treat the spin-orbit interaction in the fully relativistic four-component formalism.

Depending on cleavage plane, the (0001) surfaces of $MnBi_4Te_7$ and $MnBi_6Te_{10}$ have two and three inequivalent surface terminations, respectively, as depicted schematically in Fig. 1(c). Different surface terminations can be addressed individually by the μ-sized photon-beam spot and assigned based on a qualitative analysis of the Mn 3d spectral weight (Supplemental Material, Sec. IX [41]). ARPES data for surfaces terminated by a $MnBi_2Te_4$ septuple layer (SL) are shown in Figs. 1(a) and 1(d). For

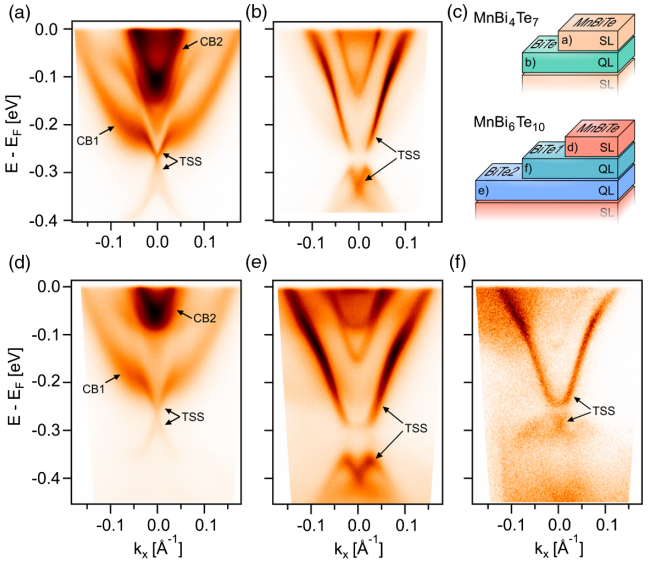

FIG. 1. Surface electronic structure for different (0001) surface terminations of $(Bi_2Te_3)_n(MnBi_2Te_4)$ with $n = 1$ and 2. (a),(b) ARPES datasets for $MnBi_4Te_7$ along $\bar{\Gamma}\bar{K}$ for a $MnBi_2Te_4$ septuple layer and a Bi_2Te_3 quintuple layer termination, respectively. (c) Schematic of the possible terminations of $MnBi_4Te_7$ and $MnBi_6Te_{10}(0001)$ surfaces, labeled with the panel showing the corresponding ARPES data. (d)–(f) ARPES datasets along $\bar{\Gamma}\bar{M}$ for $MnBi_6Te_{10}$ with (d) SL termination, (e) QL-SL termination, and (f) QL-QL termination.

both compounds we observe a qualitatively similar band structure. The main spectral features are CB1 and CB2, which we attribute to conduction band states, as well as a state with Dirac-like dispersion. We identify the latter as a topological surface state (TSS), which is in agreement with previous work [14,27,32] and confirmed by our CD-ARPES experiments discussed below. By contrast, data obtained for surfaces terminated by a Bi_2Te_3 quintuple layer (QL) do not display a clearly discernable Dirac-like dispersion [Figs. 1(b), 1(e), and 1(f)]. Instead, as we demonstrate in later parts of the Letter, the TSS dispersion is split into an upper part, whose dispersion flattens near the $\bar{\Gamma}$ point, and a lower part, whose dispersion is reminiscent of a holelike band with Rashba-type spin splitting [45]. While the general band-structure features in Fig. 1 are consistent with previous work, a precise assignment of the individual features is still controversial [31–38]. The measurements in Fig. 1 were carried out at temperatures of ca. $T \sim 11$ K, i.e., just slightly below the magnetic ordering temperatures of 12–13 K [24,26], at which no signature of a magnetic gap in the TSS could be observed.

To investigate the character of the electronic states in more detail we performed light-polarization- and photon-energy-dependent measurements. We first consider SL-terminated surfaces as studied by CD-ARPES. The CD signal is defined as the difference in photoemission intensity between right and left circularly polarized light $CD(k_x, k_y, E) = I_R(k_x, k_y, E) - I_L(k_x, k_y, E)$. It can

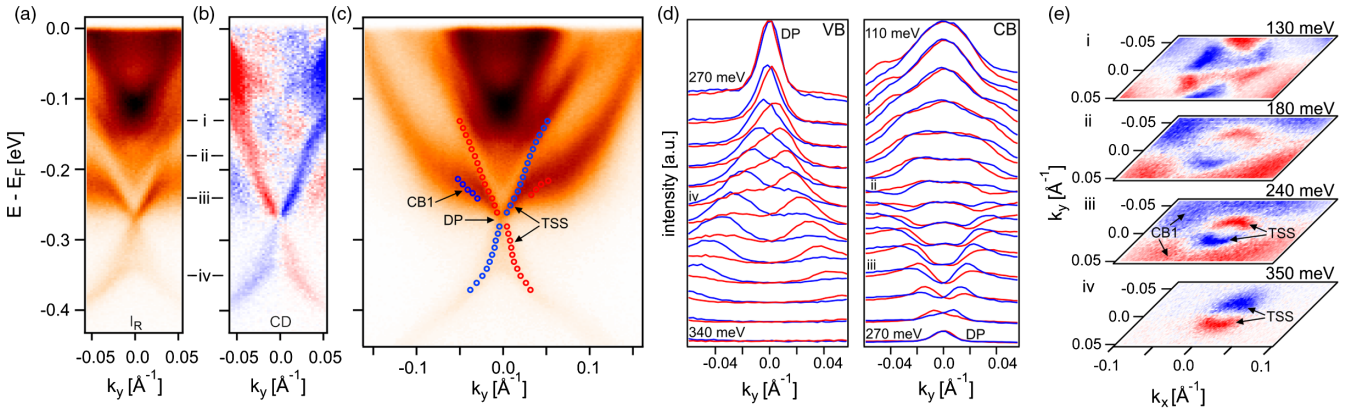

FIG. 2. CD-ARPES experiments for the SL-terminated surface of $MnBi_4Te_7$. (a) ARPES intensity I_R measured with right circularly polarized light. Wave vectors k_y are perpendicular to the plane of light incidence. (b) Corresponding CD dataset defined as the intensity difference $I_R - I_L$. (c) ARPES intensity measured with s-polarized light. The overlaid markers indicate the dispersion extracted from CD-ARPES data in (b) and the red or blue color refers to the sign of the CD. (d) Momentum distribution curves measured with right and left circularly polarized light shown in blue and red, respectively. The energy regions above and below the Dirac point (DP) are labeled by CB and VB, respectively. (e) Constant energy contours of the CD-ARPES signal.

provide detailed information about the orbital character of electronic states [46–49]. Figure 2 shows CD-ARPES data for the SL-termination of $MnBi_4Te_7$. Interestingly, as opposed to the bare ARPES intensity in Fig. 2(a), the CD spectral signature of the upper part of the TSS in Fig. 2(b) is clearly distinguished from the band CB1. This is due to the fact that these two features display opposite CD patterns, which is also seen in the constant-energy CD maps in Fig. 2(e). Consequently, the linear dispersion of the TSS can be traced to significantly higher energies than in the ARPES intensity. The TSS for the SL-terminated surface thus shows a rather ideal Dirac-cone dispersion over several hundred meV, comparable to paradigmatic TI like Bi_2Se_3 [50].

Focusing on the TSS, our data in Fig. 2 reveal a sign change of the CD at the Dirac point (DP), as indicated by the markers in Fig. 2(c). This reversal of the CD is also seen clearly in the momentum distribution curves for I_R and I_L in Fig. 2(d) and in the constant-energy contours in Fig. 2(e). The fact that the reversal occurs precisely at the energy of the DP indicates that it originates from a difference of the TSS wave function above and below the DP [47,51,52]. Indeed, previous ARPES measurements for Bi_2Se_3 identified a sign reversal of the CD at the DP as a characteristic signature of the TSS [47,53]. Specifically, the opposite CD has been shown to reflect a chiral orbital angular momentum (OAM) of opposite sign in the upper and lower part of the Dirac cone [47,54,55]. Our CD-ARPES data confirm this OAM reversal for the present MTI and thus establish the helical nature of the TSS (see also Supplemental Material, Secs. IV and V [41]). This result is complemented by spin-resolved ARPES data and calculations (see Supplemental Material, Figs. S4 and S5 [41]) that prove a chiral spin angular momentum (SAM) of the TSS.

We now turn to the electronic structure of the QL-terminated surface, where a gaplike feature modifies the dispersion of the TSS. This led to inconsistent interpretations of the topological character of the states, ranging from a gapped TSS [25–27,35], over an intact DP either at the flat part of the TSS [31,33] or at the lower Rashba-like part of the TSS [34] (cf. Fig. 1), to even more complex scenarios where DPs arise from additional nontopological surface bands [37].

Based on DFT calculations the gaplike feature has been attributed to hybridization of the TSS with states at the valence band maximum [34]. Our $h\nu$-dependent ARPES data in Fig. 3 experimentally confirm this hybridization scenario and show how it drives a complex momentum-dependent orbital-character modulation in the surface band structure. For the upper part of the TSS we observe a strong change in intensity at the "kink," where the dispersion evolves from its steeply dispersive part into the flat part close to the $\bar{\Gamma}$ point [Figs. 3(a)–3(d)]. At the valence band (VB) maximum we observe similarly abrupt intensity changes at approximately the same wave vectors. The fact that these intensity changes occur at characteristic points in the surface band structure and systematically for different photon energies shows that they reflect momentum-dependent variations of the initial state wave function, i.e., changes in the orbital composition [56,57]. Interestingly, the relative intensities of the different parts of the band structure also strongly vary with photon energy, as seen by comparing the datasets in Figs. 3(b) and 3(c) to the one in Fig. 3(d). In the light of these data we may distinguish between parts with "TSS-like" orbital character (high cross section at $h\nu = 6.3$ and 61 eV) and parts with "VB-like" orbital character (high cross section at $h\nu = 79$ eV). The measured intensity distributions thus indicate that the flat part of the upper TSS acquires a strong VB-like character, while the states close to $\bar{\Gamma}$ near the VB maximum have TSS-like character close to the surface. This assignment is

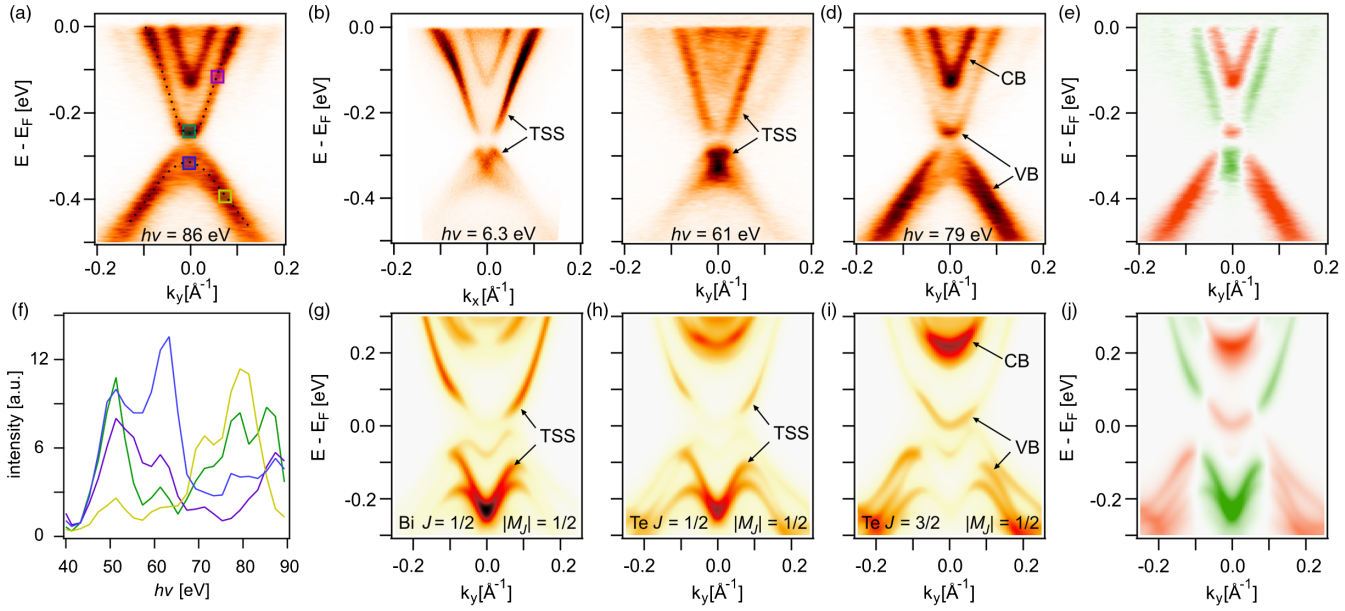

FIG. 3. (a)–(d) Photon-energy-dependent ARPES data along $\bar{\Gamma}\bar{\mathrm{K}}$ for the QL-terminated surface of $MnBi_4Te_7$ obtained with p-polarized light, except for (b) measured with s polarization [$T = 8$ K]. (e) Intensity difference between datasets measured at $h\nu = 61$ and $h\nu = 79$ eV. (f) ARPES intensities traced as a function of $h\nu$ at specific points in the band structure, indicated by boxes in (a). The colors of the boxes in (a) correspond to the respective data sets in (f). (g)–(j) Orbital-projected surface spectral densities for the QL-terminated surface of $MnBi_4Te_7$. (j) Difference between the surface spectral densities projected on Bi $J = 1/2$ orbitals in (g) and Te $J = 3/2$, $|M_J| = 1/2$ orbitals in (i).

further confirmed by the data in Fig. 3(f), showing that the measured intensities of TSS-like and VB-like parts of the band structure exhibit different characteristic $h\nu$ dependences. The data in Fig. 3(f) were normalized according to the beam line flux curve published in Ref. [58].

The observed orbital-character changes as a result of hybridization are supported by our calculations [Figs. 3(g)–3(j)]. We have simulated atom- and orbital-projected surface spectral densities by assuming an exponential decay from the surface ($\lambda = 10$ Å), reflecting qualitatively the finite probing depth of the ARPES experiment (Supplemental Material, Fig. S1 [41]). First, our simulation nicely reproduces the gaplike feature in the surface spectral density, which is independent of orbital-type and thus attributed mainly to the surface sensitivity of the experiment. This is consistent with our ARPES data where a gaplike feature is always observed, independently of $h\nu$. Second, we find qualitatively good similarities between specific orbital projections and the ARPES intensity distributions. The close correspondence to the data allows us to identify TSS-like parts of the surface band structure to arise mainly from Bi and Te $J = 1/2$ states, while the VB-like parts and also the CB can be attributed mainly to Te $J = 3/2$, $|M_J| = 1/2$ character. The difference in orbital composition of the respective band-structure parts results in distinct $h\nu$-dependent cross sections, which allows us to distinguish them in our ARPES data [Figs. 3(b)–3(d)]. The agreement between measurement and calculations is further illustrated by the difference datasets in Figs. 3(e) and 3(j), where TSS-like parts appear in green and VB- and CB-like parts appear in red. Based on this detailed analysis, the DP of the TSS can be assigned to the Rashba-like band near the VB maximum.

The topological classification of the surface bands for the QL termination is confirmed by spin-resolved ARPES data and calculations (Fig. 4). Both, experiment and theory reveal a high in-plane spin polarization for TSS-like bands. The chiral spin texture is imaged in full momentum space in the constant energy map in Fig. 4(d). Moreover, the sign of the spin polarization above and directly below the gaplike feature is found to coincide [Fig. 4(c)], further substantiating the assignment discussed above. Further, we find experimentally and theoretically a spin polarization in the conduction band states whose sign is reversed compared to the TSS spin. The same phenomenon has been observed for the nonmagnetic TI Bi_2Se_3 and attributed to surface-resonance formation [59].

The results in Figs. 3 and 4 prove that the DP lies within the region of projected bulk valence states for the QL termination. By contrast, a free-standing Dirac cone is realized in the bulk gap for the SL termination (Fig. 2). These findings bear direct relevance for the possibility of realizing a half-integer Hall conductivity $\sigma_{xy} = \pm\frac{1}{2}e^2/h$ on these surfaces. Specifically, our results indicate that a half-quantized Hall conductivity can be achieved for SL-terminated surfaces, in line with recent experiments for $MnBi_2Te_4$ [19,20]. For QL-terminated surfaces, however, the edge states will inevitably locate in the projected bulk

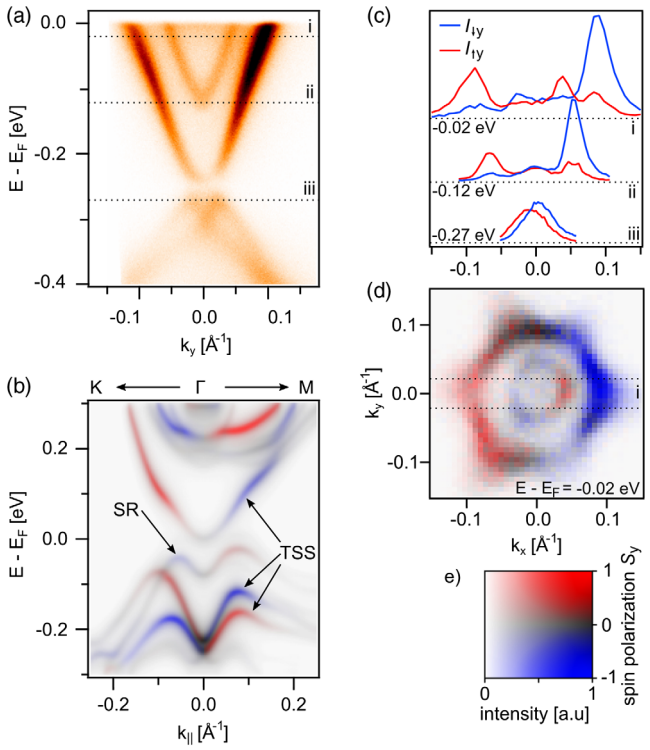

FIG. 4. (a) ARPES data along $\bar{\Gamma}\bar{\mathrm{K}}$ for QL-terminated $MnBi_4Te_7$. Dashed lines indicate the energies of the momentum distribution curves (MDC) in (c). (b) Calculated surface spectral density along $\bar{\mathrm{M}}\bar{\Gamma}\bar{\mathrm{K}}$. The intensity represents the projection on Bi and Te $J = 1/2$ orbitals and red or blue colors denote the spin polarization perpendicular to $k_{||}$. The TSS and a surface resonance (SR) are indicated. (c) MDC of the spin-resolved intensities $I_{\uparrow y}$ and $I_{\downarrow y}$ at energies (i)–(iii) indicated in (a). (d) Spin-resolved constant energy contour at energy (i). The spin quantization is along y. Dashed lines indicate the integration width used to obtain the MDC in (c). (e) Color matrix used for the simultaneous depiction of intensity and spin polarization S_y.

continuum, prohibiting a half-quantized Hall conductivity independently of the position of the Fermi level [60] (see also Supplemental Material, Fig. S6 [41]).

In conclusion, our orbital- and spin-resolved analysis enables an unequivocal assignment of the topological surface bands in the magnetic van der Waals materials $(Bi_2Te_3)_n(MnBi_2Te_4)$ ($n = 1$ and 2), and it establishes the helical nature of the surface states. An ideal surface Dirac cone is observed for $MnBi_2Te_4$-terminated surfaces. For Bi_2Te_3-terminated surfaces, hybridization with valence-band states yields a more complex band structure, with a nonmagnetic gaplike feature in the surface spectral weight and the surface-state Dirac point buried in the bulk continuum. These distinct electronic features for different surface terminations will be directly relevant to realizing long-sought topological phenomena in $MnBi_2Te_4$-based van der Waals compounds, such as axion electrodynamics, Majorana fermions, or higher-order topology. Our results also indicate that structure-property relations in van der Waals heterostructures, e.g., several possible terminations of a single bulk compound, can be exploited to modify the topological electronic surface properties.

We acknowledge financial support from the DFG through SFB1170 "Tocotronics" (Project A01), SFB1143 "Correlated Magnetism," RE1469/13-1, SPP 1666 "Topological insulators" (IS 250/1-2 and PL 712/2-1), ERA-Chemistry Programm (RU-776/15-1), and the Würzburg-Dresden Cluster of Excellence on Complexity and Topology in Quantum Matter—*ct.qmat* (EXC 2147, project-id 390858490). Part of this work was carried out with the support of the Diamond Light Source, beam line I05 (Proposal No. SI22468-1). Part of the ARPES measurements were performed with the approval of the Proposal Assessing Committee of the Hiroshima Synchrotron Radiation Center (Proposal No. 19BU010). We thank Ulrike Nitzsche for assistance regarding high-performance compute facilities at IFW. The work received funding from the DFG under Germany's Excellence Strategy–Cluster of Excellence Matter and Light for Quantum Computing (ML4Q) EXC 2004/1-390534769. M. R. and J. I. F. are thankful to Arthur Ernst for useful correspondence. J. I. F. acknowledges the support from the Alexander von Humboldt Foundation.

*Hendrik.Bentmann@physik.uni-wuerzburg.de

[1] R. Yu, W. Zhang, H.-J. Zhang, S.-C. Zhang, X. Dai, and Z. Fang, Science **329**, 61 (2010).
[2] C.-Z. Chang, J. Zhang, X. Feng, J. Shen, Z. Zhang, M. Guo, K. Li, Y. Ou, P. Wei, L.-L. Wang *et al.*, Science **340**, 167 (2013).
[3] D. F. Liu, A. J. Liang, E. K. Liu, Q. N. Xu, Y. W. Li, C. Chen, D. Pei, W. J. Shi, S. K. Mo, P. Dudin *et al.*, Science **365**, 1282 (2019).
[4] M. M. Otrokov, I. I. Klimovskikh, H. Bentmann, D. Estyunin, A. Zeugner, Z. S. Aliev, S. Ga, A. U. B. Wolter, A. V. Koroleva, A. M. Shikin *et al.*, Nature (London) **576**, 416 (2019).
[5] E. D. L. Rienks, S. Wimmer, J. Snchez-Barriga, O. Caha, P. S. Mandal, J. Rika, A. Ney, H. Steiner, V. V. Volobuev, H. Groiss *et al.*, Nature (London) **576**, 423 (2019).
[6] C.-Z. Chang, W. Zhao, D. Y. Kim, H. Zhang, B. A. Assaf, D. Heiman, S.-C. Zhang, C. Liu, M. H. W. Chan, and J. S. Moodera, Nat. Mater. **14**, 473 (2015).
[7] S. Grauer, K. M. Fijalkowski, S. Schreyeck, M. Winnerlein, K. Brunner, R. Thomale, C. Gould, and L. W. Molenkamp, Phys. Rev. Lett. **118**, 246801 (2017).
[8] D. Xiao, J. Jiang, J.-H. Shin, W. Wang, F. Wang, Y.-F. Zhao, C. Liu, W. Wu, M. H. W. Chan, N. Samarth *et al.*, Phys. Rev. Lett. **120**, 056801 (2018).
[9] Y. Gong, J. Guo, J. Li, K. Zhu, M. Liao, X. Liu, Q. Zhang, L. Gu, L. Tang, X. Feng *et al.*, Chin. Phys. Lett. **36**, 076801 (2019).
[10] R. C. Vidal, H. Bentmann, T. R. F. Peixoto, A. Zeugner, S. Moser, C.-H. Min, S. Schatz, K. Kißner, M. Ünzelmann, C. I. Fornari *et al.*, Phys. Rev. B **100**, 121104 (2019).

[11] B. Chen, F. Fei, D. Zhang, B. Zhang, W. Liu, S. Zhang, P. Wang, B. Wei, Y. Zhang, Z. Zuo *et al.*, Nat. Commun. **10**, 4469 (2019).

[12] Y.-J. Hao, P. Liu, Y. Feng, X.-M. Ma, E. F. Schwier, M. Arita, S. Kumar, C. Hu, R. Lu, M. Zeng *et al.*, Phys. Rev. X **9**, 041038 (2019).

[13] Y. J. Chen, L. X. Xu, J. H. Li, Y. W. Li, H. Y. Wang, C. F. Zhang, H. Li, Y. Wu, A. J. Liang, C. Chen *et al.*, Phys. Rev. X **9**, 041040 (2019).

[14] H. Li, S.-Y. Gao, S.-F. Duan, Y.-F. Xu, K.-J. Zhu, S.-J. Tian, J.-C. Gao, W.-H. Fan, Z.-C. Rao, J.-R. Huang *et al.*, Phys. Rev. X **9**, 041039 (2019).

[15] P. Swatek, Y. Wu, L.-L. Wang, K. Lee, B. Schrunk, J. Yan, and A. Kaminski, Phys. Rev. B **101**, 161109(R) (2020).

[16] H. Deng, Z. Chen, A. Wolo, M. Konczykowski, K. Sobczak, J. Sitnicka, I. V. Fedorchenko, J. Borysiuk, T. Heider, L. Plucinski *et al.*, Nat. Phys. **17**, 36 (2021).

[17] M. M. Otrokov, T. V. Menshchikova, M. G. Vergniory, I. P. Rusinov, A. Y. Vyazovskaya, Y. M. Koroteev, G. Bihlmayer, A. Ernst, P. M. Echenique, A. Arnau *et al.*, 2D Mater. **4**, 025082 (2017).

[18] M. M. Otrokov, I. P. Rusinov, M. Blanco-Rey, M. Hoffmann, A. Y. Vyazovskaya, S. V. Eremeev, A. Ernst, P. M. Echenique, A. Arnau, and E. V. Chulkov, Phys. Rev. Lett. **122**, 107202 (2019).

[19] Y. Deng, Y. Yu, M. Z. Shi, Z. Guo, Z. Xu, J. Wang, X. H. Chen, and Y. Zhang, Science **367**, 895 (2020).

[20] C. Liu, Y. Wang, H. Li, Y. Wu, Y. Li, J. Li, K. He, Y. Xu, J. Zhang, and Y. Wang, Nat. Mater. **19**, 522 (2020).

[21] D. Zhang, M. Shi, T. Zhu, D. Xing, H. Zhang, and J. Wang, Phys. Rev. Lett. **122**, 206401 (2019).

[22] J. Li, Y. Li, S. Du, Z. Wang, B.-L. Gu, S.-C. Zhang, K. He, W. Duan, and Y. Xu, Sci. Adv. **5**, eaaw5685 (2019).

[23] Z. S. Aliev, I. R. Amiraslanov, D. I. Nasonova, A. V. Shevelkov, N. A. Abdullayev, Z. A. Jahangirli, E. N. Orujlu, M. M. Otrokov, N. T. Mamedov, M. B. Babanly *et al.*, J. Alloys Compd. **789**, 443 (2019).

[24] D. Souchay, M. Nentwig, D. Gnther, S. Keilholz, J. d. Boor, A. Zeugner, A. Isaeva, M. Ruck, A. U. B. Wolter, B. Bchner *et al.*, J. Mater. Chem. C **7**, 9939 (2019).

[25] J. Wu, F. Liu, M. Sasase, K. Ienaga, Y. Obata, R. Yukawa, K. Horiba, H. Kumigashira, S. Okuma, T. Inoshita *et al.*, Sci. Adv. **5**, eaax9989 (2019).

[26] R. C. Vidal, A. Zeugner, J. I. Facio, R. Ray, M. H. Haghighi, A. U. B. Wolter, L. T. Corredor Bohorquez, F. Caglieris, S. Moser, T. Figgemeier *et al.*, Phys. Rev. X **9**, 041065 (2019).

[27] C. Hu, K. N. Gordon, P. Liu, J. Liu, X. Zhou, P. Hao, D. Narayan, E. Emmanouilidou, H. Sun, Y. Liu *et al.*, Nat. Commun. **11**, 97 (2020).

[28] Y. Peng and Y. Xu, Phys. Rev. B **99**, 195431 (2019).

[29] R.-X. Zhang, F. Wu, and S. Das Sarma, Phys. Rev. Lett. **124**, 136407 (2020).

[30] H. Sun, B. Xia, Z. Chen, Y. Zhang, P. Liu, Q. Yao, H. Tang, Y. Zhao, H. Xu, and Q. Liu, Phys. Rev. Lett. **123**, 096401 (2019).

[31] L. X. Xu, Y. H. Mao, H. Y. Wang, J. H. Li, Y. J. Chen, Y. Y. Y. Xia, Y. W. Li, J. Zhang, H. J. Zheng, K. Huang *et al.*, Sci. Bull. **65**, 2086 (2020).

[32] Y. Hu, L. Xu, M. Shi, A. Luo, S. Peng, Z. Y. Wang, J. J. Ying, T. Wu, Z. K. Liu, C. F. Zhang *et al.*, Phys. Rev. B **101**, 161113(R) (2020).

[33] S. Tian, S. Gao, S. Nie, Y. Qian, C. Gong, Y. Fu, H. Li, W. Fan, P. Zhang, T. Kondo *et al.*, Phys. Rev. B **102**, 035144 (2020).

[34] I. I. Klimovskikh, M. M. Otrokov, D. Estyunin, S. V. Eremeev, S. O. Filnov, A. Koroleva, E. Shevchenko, V. Voroshnin, A. G. Rybkin, I. P. Rusinov *et al.*, npj Quantum Mater. **5**, 54 (2020).

[35] K. N. Gordon, H. Sun, C. Hu, A. G. Linn, H. Li, Y. Liu, P. Liu, S. Mackey, Q. Liu, N. Ni *et al.*, arXiv:1910.13943.

[36] N. H. Jo, L.-L. Wang, R.-J. Slager, J. Yan, Y. Wu, K. Lee, B. Schrunk, A. Vishwanath, and A. Kaminski, Phys. Rev. B **102**, 045130 (2020).

[37] X.-M. Ma, Z. Chen, E. F. Schwier, Y. Zhang, Y.-J. Hao, R. Lu, J. Shao, Y. Jin, M. Zeng, X.-R. Liu *et al.*, Phys. Rev. B **102**, 245136 (2020).

[38] X. Wu, J. Li, X.-M. Ma, Y. Zhang, Y. Liu, C.-S. Zhou, J. Shao, Q. Wang, Y.-J. Hao, Y. Feng *et al.*, Phys. Rev. X **10**, 031013 (2020).

[39] H. Iwasawa, E. F. Schwier, M. Arita, A. Ino, H. Namatame, M. Taniguchi, Y. Aiura, and K. Shimada, Ultramicroscopy **182**, 85 (2017).

[40] M. Hoesch, T. Kim, P. Dudin, H. Wang, S. Scott, P. Harris, S. Patel, M. Matthews, D. Hawkins, S. Alcock *et al.*, Rev. Sci. Instrum. **88**, 013106 (2017).

[41] See Supplemental Material at http://link.aps.org/supplemental/10.1103/PhysRevLett.126.176403 for additional methodological details and supporting experimental and theoretical results.

[42] J. P. Perdew, K. Burke, and M. Ernzerhof, Phys. Rev. Lett. **77**, 3865 (1996).

[43] K. Koepernik and H. Eschrig, Phys. Rev. B **59**, 1743 (1999).

[44] https://www.fplo.de/.

[45] H. Maaß, H. Bentmann, C. Seibel, C. Tusche, S. V. Eremeev, T. R. F. Peixoto, O. E. Tereshchenko, K. A. Kokh, E. V. Chulkov, J. Kirschner *et al.*, Nat. Commun. **7**, 11621 (2016).

[46] G. Schönhense, C. Westphal, J. Bansmann, M. Getzlaff, J. Noffke, and L. Fritsche, Surf. Sci. **251–252**, 132 (1991).

[47] S. R. Park, J. Han, C. Kim, Y. Y. Koh, C. Kim, H. Lee, H. J. Choi, J. H. Han, K. D. Lee, N. J. Hur *et al.*, Phys. Rev. Lett. **108**, 046805 (2012).

[48] J. Sánchez-Barriga, A. Varykhalov, J. Braun, S.-Y. Xu, N. Alidoust, O. Kornilov, J. Minár, K. Hummer, G. Springholz, G. Bauer *et al.*, Phys. Rev. X **4**, 011046 (2014).

[49] V. Sunko, H. Rosner, P. Kushwaha, S. Khim, F. Mazzola, L. Bawden, O. J. Clark, J. M. Riley, D. Kasinathan, M. W. Haverkort *et al.*, Nature (London) **549**, 492 (2017).

[50] Y. Xia, D. Qian, D. Hsieh, L. Wray, A. Pal, H. Lin, A. Bansil, D. Grauer, Y. S. Hor, R. J. Cava *et al.*, Nat. Phys. **5**, 398 (2009).

[51] Y. Cao, J. A. Waugh, X.-W. Zhang, J.-W. Luo, Q. Wang, T. J. Reber, S. K. Mo, Z. Xu, A. Yang, J. Schneeloch *et al.*, Nat. Phys. **9**, 499 (2013).

[52] H. Zhang, C.-X. Liu, and S.-C. Zhang, Phys. Rev. Lett. **111**, 066801 (2013).

[53] Y. H. Wang, D. Hsieh, D. Pilon, L. Fu, D. R. Gardner, Y. S. Lee, and N. Gedik, Phys. Rev. Lett. **107**, 207602 (2011).

[54] J.-H. Park, C. H. Kim, J.-W. Rhim, and J. H. Han, Phys. Rev. B **85**, 195401 (2012).
[55] S. R. Park and C. Kim, J. Electron Spectrosc. Relat. Phenom. **201**, 6 (2015).
[56] H. Bentmann, S. Abdelouahed, M. Mulazzi, J. Henk, and F. Reinert, Phys. Rev. Lett. **108**, 196801 (2012).
[57] C.-H. Min, H. Bentmann, J. N. Neu, P. Eck, S. Moser, T. Figgemeier, M. Ünzelmann, K. Kissner, P. Lutz, R. J. Koch *et al.*, Phys. Rev. Lett. **122**, 116402 (2019).
[58] M. Hoesch, T. Kim, P. Dudin, H. Wang, S. Scott, P. Harris, S. Patel, M. Matthews, D. Hawkins, S. Alcock *et al.*, Rev. Sci. Instrum. **88**, 013106 (2017).
[59] C. Jozwiak, J. A. Sobota, K. Gotlieb, A. F. Kemper, C. R. Rotundu, R. J. Birgeneau, Z. Hussain, D.-H. Lee, Z.-X. Shen, and A. Lanzara, Nat. Commun. **7**, 13143 (2016).
[60] K. Nomura and N. Nagaosa, Phys. Rev. Lett. **106**, 166802 (2011).

Correction: A proof change request for the affiliation list was mishandled and resulted in the wrong assignment of affiliation numbers for author A. Isaeva, which has now been set right.

Second Correction: The omission of a support statement in the Acknowledgments section has been fixed.